EXPERIMENTAL INVESTIGATION OF BUBBLE NUCLEATION, GROWTH AND DEPARTURE USING SYNCHRONIZED IR THERMOMETRY, TWO-COLOUR LIF AND PIV

Gustavo M. Aguiar[1], Victor Voulgaropoulos[2], Omar K. Matar[2], Christos N. Markides[2,+], Matteo Bucci[1,*]

[1] Department of Nuclear Science and Engineering
Massachusetts Institute of Technology
77 Massachusetts Avenue, Cambridge MA, USA
* mbucci@mit.edu

[2] Department of Chemical Engineering
Imperial College London
London SW7 2AZ, UK
+ c.markides@imperial.ac.uk

ABSTRACT

Boiling is a very effective heat removal process exploited in many applications, from electronic devices to nuclear reactors. However, the physical mechanisms involved in this process are not fully understood yet, due to its complexity, which arises from the many interacting sub-processes involved in the nucleation, growth, and detachment of isolated bubbles. Here, we present the methodology and initial results from an experimental investigation aimed at elucidating and quantifying the mechanisms involved in a bubble life cycle (from nucleation until departure). Towards this aim, we use synchronized high-speed infrared (IR) thermometry, ratiometric two-color laser-induced fluorescence (2cLIF) and particle image velocimetry (PIV). Infrared thermometry is used to measure the time-dependent temperature and heat flux distributions over the boiling surface, which are useful to quantify the transfer of energy associated with the evaporation of the micro-layer. Two-color laser-induced fluorescence is used to measure the time-dependent temperature distribution in the liquid phase. Particle image velocimetry is employed to measure the velocity field around the bubble, necessary to elucidate the bubble growth and departure mechanisms. The investigation also reveals other fundamental heat transfer aspects such as the dynamics of the near-wall superheated liquid layer, the mixing effect produced by bubble growth and departure, as well as convection effects around the bubble.

KEYWORDS
2cLIF, Bubble life cycle, IR thermometry, PIV

1. INTRODUCTION

Boiling is a highly-efficient mode of heat transfer due to latent heat transport. Thus, its use is favored in many demanding industrial applications such as the heat removal from a nuclear reactor core and the direct steam generation in solar systems [1]. Despite the widespread use of boiling in several industrial processes, the role of the several interacting physical mechanisms involved in the nucleation, growth, and detachment of vapor bubbles and their individual impact on the overall heat transfer efficiency is still not

clear. As a result, many of the methods commonly used to predict boiling heat removal performance are still predominantly empirical and their accuracy is inherently restricted to a narrow range of operational conditions. The rapid technological progress of the electronics industry experienced over the last decades certainly facilitated the improvement of the temporal and spatial resolution of many fluid diagnostics techniques such as infrared thermometry [2] and laser-induced fluorescence [3–6]. The increasing level of detail captured by these advanced fluid diagnostic techniques provide valuable benchmark data for numerical modeling validations and can potentially aid in the development of more accurate mechanistic models for predicting heat transfer behavior.

Within this context, this paper presents the methodology and some initial findings from the investigation of single vapor bubbles nucleating from pool boiling water at atmospheric pressure. We combined the simultaneous use of different advanced high-speed optical and infrared diagnostic techniques. Ratiometric two-color laser-induced fluorescence (2cLIF) and particle image velocimetry (PIV) techniques were used to measure the liquid-phase temperature and velocity field, respectively, and infrared thermometry (IR) was used to measure the temperature and heat flux distributions on the boiling surface. The results enabled us to quantify essential aspects related to thermal energy transfer such as the dynamics of the near-wall superheated liquid layer.

2. EXPERIMENTAL METHODOLOGY

2.1. Experimental Apparatus

The experimental apparatus and the instrumentation employed during the nucleate boiling experiments are schematically illustrated in Fig. 1. The boiling cell was filled with deionized (DI) water and brought to its saturation temperature at atmospheric pressure by circulating a warm bath fluid. The water temperature was monitored by two K-type thermocouples. Four sapphire windows symmetrically distributed around the heater laterals provided optical access to the high-speed video (HSV) cameras and the laser sheet. An IR camera was used to measure the temperature distribution across the ITO heater from the bottom of the cell, as shown in Fig. 1.

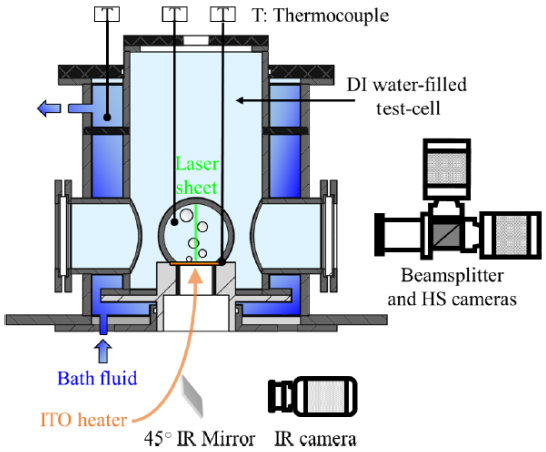


Figure 1. Schematics of the boiling cell and the instrumentation used during experiments.

An ITO coating of 700 nm thickness opaque to the 3 – 5 µm wavelength range was deposited on top of a 1 mm thick and 20 × 20 mm^2 sapphire substrate to serve as a Joule-effect heater in direct contact with the fluid. Silver pads were deposited on top of the ITO coating to provide electrical connections necessary to uniformly power the heater while defining an active area of 10 × 10 mm^2. In this study, it was imperative to fix the position of a single nucleation site in order to avoid multiple bubble interactions and minimize

the misalignments between the laser light sheet plane and the bubble center. To accomplish this goal, a small square region of 100 × 100 μm^2 dimensions was coated with a hydrophobic polymer (PTFE) to serve as an artificial nucleation site at the central portion of the heater.

2.2. Liquid Temperature and Velocity Diagnostics

A ratiometric 2cLIF method was used to obtain the temperature distribution of the liquid phase during the tests. A laser light sheet excited two fluorescent dyes, namely Fluorescein disodium (FL) and Sulforhodamine 101 (SR). The intensity of the SR fluorescence is independent of the local temperature, while the fluorescence intensity of FL increases with temperature. By tracking the ratio of the light intensity emission from the two dyes, it is possible to reconstruct the temperature field of the liquid phase, particularly close to the bubble interface, where light reflections were present. A similar method was employed by Chaze et al. [7] to measure the temperature field inside of liquid droplets impinging on a hot solid surface. The FL and SR dyes were dissolved in water with molar concentrations of $4 \cdot 10^{-5}$ M and $1.4 \cdot 10^{-7}$ M, respectively. Additionally, fluorescent tracer particles with a 10 μm mean diameter, emitting primarily 550 nm were seeded to the water in concentrations below 10^{-2} M to enable PIV measurements. Two high-speed video cameras were attached to a pellicle beam splitter (reflectivity 45%: transmissivity 55%) mounted with a Nikon 105 mm lens. Appropriate optical filters (combinations of notch, high-pass and band-pass) were mounted inside the extension tubes connecting each camera to the beam splitter, and their use permitted the monitoring of the fluorescent signal of each dye separately. Figure 2 illustrates the emission/absorption spectral bands of the fluorescent dyes and the range recorded by the high-speed video cameras. Precisely, the first camera, CAM_{FL} (Phantom V12.1), recorded the intensity of the temperature-sensitive FL dye (Band 1 in Fig. 2), while the second camera, CAM_{SR} (Phantom V25.12), recorded the intensity of the temperature insensitive SR dye (Band 2 in Fig. 2). The spectral bands of each camera were carefully selected to avoid spectral conflicts, which can lead to erroneous temperature measurements [8].

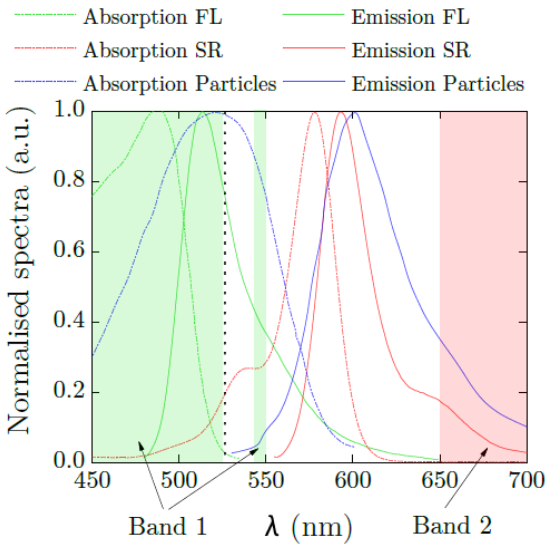


Figure 2. Emission/absorption spectral bands of fluorescent dyes and cameras optical filters spectral bands. λ is the light wavelength.

A single cavity of a pulsed high-speed Nd: YLF laser (527 nm) operating at 2.5 kHz and with a current of 30 A was used to excite the two fluorescent dyes and the particles. Dedicated optics were connected to the laser head to generate a thin sheet of light of an experimentally determined thickness equal to 211 μm. It has been shown that SR is subjected to thermal degradation for temperatures higher than the ambient

(>30 °C) [7]. In this study, we quantified the SR thermal degradation prior to the pool boiling experiments. A solution of DI Water and SR was brought to 98 °C and the normalized light intensity was monitored for approximately two hours while maintaining the temperature constant. The results revealed that the fluorescence intensity decreased linearly with time at a rate of approximately -40%/hour. The time elapsed from the introduction of the dyes in the heated water until the completion of data acquisition and calibration was kept under 30 min. The empirically determined thermal degradation rate was used to compensate the SR signal attenuation during the post-processing of the 2cLIF data. The reader is referred to our previous paper [9] for a thorough description of the liquid temperature measurements using the 2cLIF technique.

Spatial calibration and image corrections were applied to the 2cLIF and PIV images using in-built functions of DaVis 8.4 (LaVision) and in-house developed MATLAB (Mathworks) algorithms. For the 2cLIF technique, the images from both cameras need to have a matching field of view with a pixel to pixel correspondence. Images of a calibration target with patterned circles of known distances and dimensions immersed in the cell were taken and the native spatial calibration algorithm of DaVis 8.4 was applied to the raw image to minimize any rotation/magnification differences between the two HSV cameras, providing a pixel resolution of 52 μm. Also, the PIV seeding particles were removed from the LIF images using a similar method described by Voulgaropoulos and Angeli [10]. To obtain the velocity field in the water phase, a methodology analogous to Charogiannis et al. [11] was employed to mask out the vapor phase and prevent erroneous calculation of velocity vectors in this phase. The DaVis 8.4 PIV cross-correlation algorithm was used in a three-pass iterative mode with interrogation windows of decreasing size, starting from 64 by 64 pixels^2 towards 32 by 32 pixels^2 with 50% overlap. The images are post-processed with a universal outlier detection and any windows containing outliers were emptied and interpolated. Finally, the optimal smoothing filter of DaVis 8.4 was applied.

2.3. Infrared Temperature Diagnostics of the Heater

A high-speed infrared camera (TELOPS Fast M3k) mounted with a 100 mm lens was used to record the thermal radiation emitted by the boiling surface during the experiments at a spatial resolution of 50 μm per pixel and 2500 frames per second. The total radiation measured by the IR camera is a combination of the radiation emitted by the ITO heater, the sapphire substrate, and the reflections of the background radiation. The sapphire substrate is semi-transparent in the IR range (3.5 to 5 μm) and its absorption coefficient is highly dependent on the IR radiation wavelength, resulting in non-uniform and time-dependent contamination of the primary radiation of the ITO heater. Also, part of the power supplied to the heater is not directed to the fluid, but lost to the sapphire substrate, which exhibits good thermal conductivity and thermal capacity. To account for these effects, the mechanistic procedure developed by Bucci et al. [12] was used to accurately estimate the temperature and the heat flux distributions on the boiling surface. In this technique, an inverse coupled 3D heat conduction/2D radiation problem is iteratively calculated to resolve the temperature and heat flux distributions at the heater surface. The reader is referred to Ref. [12] for a comprehensive description of the IR temperature diagnostics procedure adopted in this study.

3. RESULTS

Single bubble experiments were carried out for nominal heat flux ranging from 30 to 60 kW/m² under atmospheric pressure. For nominal heat fluxes higher than 60 kW/m², it was found that the occurrence of multiple nucleation sites throughout the heater and their interference in the laser light path limited the applicability of the 2cLIF technique, as illustrated in Fig. 3. In this paper, we show results for a nominal heat flux of 30 kW/m². For this condition, the onset of nucleate boiling on top of the artificial nucleation site (PTFE coating) occurred for wall superheat temperatures of approximately 6.7 °C. Also, it was observed that the wait time, defined as the time between bubble departure and the nucleation of the next

bubble, had an average value of 8 ms while the growth time, defined as the time from bubble nucleation to departure, had an average value of 20 ms. Bubble departure frequencies ranging from 30 to 40 Hz were recorded.

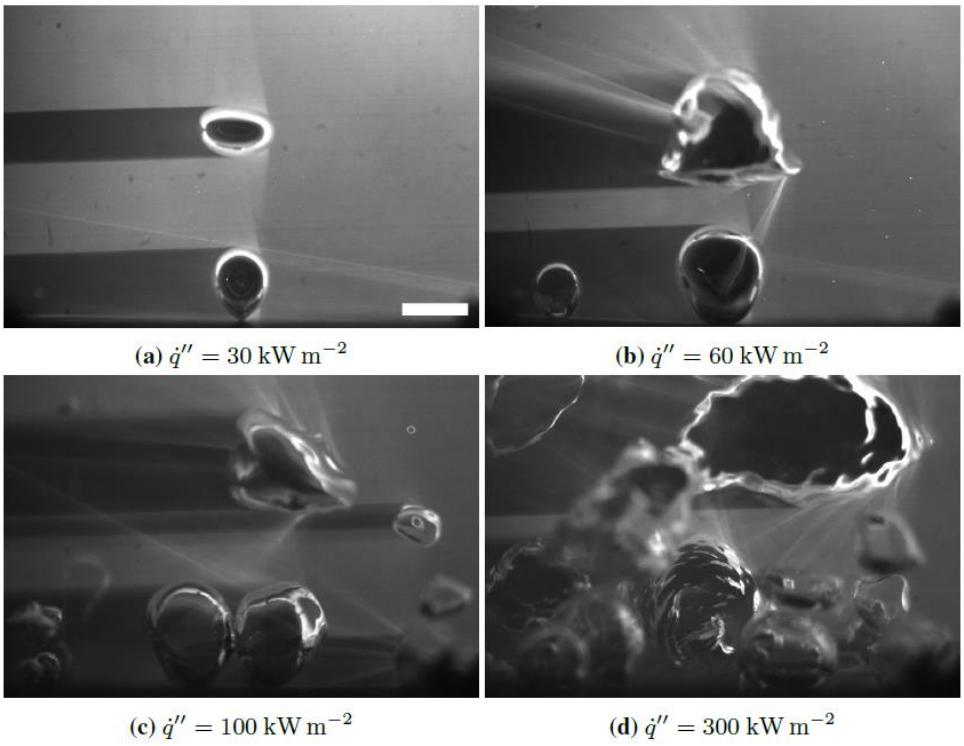


Figure 3. Illustration of the limitations of 2cLIF technique at high heat fluxes due to the occurrence of multiple nucleation sites. The scale bar corresponds to 2 mm.

A linearly increasing relationship between the ratio of the fluorescent of both dyes and the temperature of water was found for temperatures ranging from 85 °C to 100 °C, measured as the mean of the two K-type thermocouples (0.5 °C error) placed within the boiling cell (see Fig. 1). The fluorescence intensities recorded by CAM_{FL} and CAM_{SR} (I_{FL} and I_{SR}, respectively) were obtained from the spatial average over the area of interest and time average over 300 frames. A linear curve fitting between the reference temperature and the dyes fluorescence intensity ratio given by $I_R = I_{FL}/ I_{SR}$ provided an analytical expression for estimating the temperatures. The sensitivity of the 2cLIF measurements was estimated as the inverse of the slope of the fitted line ($R^2 = 0.98$), resulting in approximately 1% per °C.

Liquid-phase temperature fields obtained from the 2cLIF technique and the corresponding velocity fields obtained from the PIV technique are shown in Fig. 4 for five typical time-steps during one bubble life cycle at 30 kW/m². In this figure, the vapor-phase is represented by the blue region and each contour level corresponds to a 0.5 °C temperature change. The time instant $t^* = 0$ ms was referenced as the first frame where a nucleating bubble was recorded. The temperature fields from Fig. 4 reveal the presence of a superheated liquid layer at approximately 102 °C close to the nucleation site region. Also, it is seen from Fig. 4(e) that a thin superheated liquid layer remains in contact with the liquid-vapor interface after the bubble nucleates and expands. All these observations are consistent with the findings from Narayan et al. [13], which used the rainbow Schlieren technique to visualize the temperature field around single bubble nucleation at similar conditions.

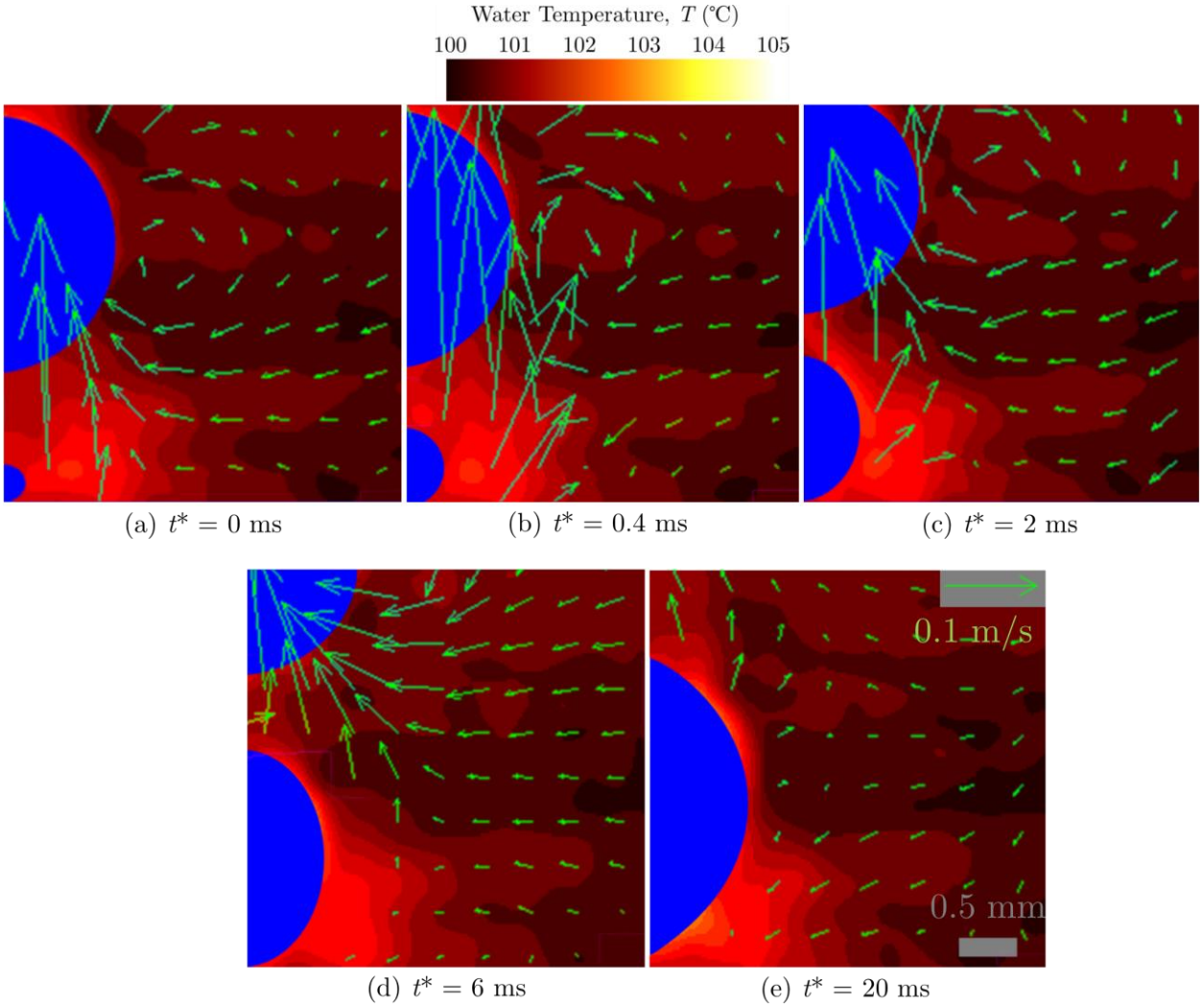


Figure 4. Temperature (2cLIF) and velocity (PIV) fields around a vapor bubble from nucleation to departure under a nominal heat flux of 30 kW/m² and T_{sat} = 100 °C. The blue region represents the vapor phase and each temperature contour level corresponds to 0.5 °C.

The liquid mixing effect induced by the bubble growth and departure is clearly verified in Fig. 4. The combined motions from the wake region generated by the rise of the previous bubble and the rapid expansion of the vapor-liquid interface of the growing bubble displace upwards a fraction of the superheated liquid layer initially in contact with the wall. This effect produced by the bubble growth and departure results in an accumulation of superheated liquid close to the nucleation site. It is worth mentioning that the accumulation of superheated liquid adjacent to the nucleation site should facilitate the nucleation of the next bubble, thus the recirculation flow structures contribute to the overall nucleation process. Unfortunately, we were not able to observe a natural convection thermal boundary layer at the heater vicinity. An ongoing effort is being made to improve the temperature measurement sensitivity and spatial resolution to a level which will enable us to compute the heat transfer from the superheated liquid layer to the vapor phase.

Figure 5 shows the heat flux and temperature distributions obtained from the post-processing of the IR images. From Fig. 5(a), it is verified that the heat flux promptly increases as soon as the bubble is generated. Moreover, local heat fluxes as high as 600 kW/m² (Fig. 5(c)) were recorded during the initial

stages of the bubble growth. The explanation for the large differences between the peak and nominal heat flux (30 kW/m²) resides on the heat transfer efficiency promoted by the microlayer evaporation. During the initial stages of bubble growth, the vapor-liquid interface rapidly moves outwards and a thin layer of liquid of few microns thick is trapped underneath the bubble. This liquid layer is known as the microlayer and it exhibits low thermal resistance owing to the heat conduction through the thin liquid film. It is worth mentioning that, under this study conditions, bubble departure was observed before the microlayer depletion.

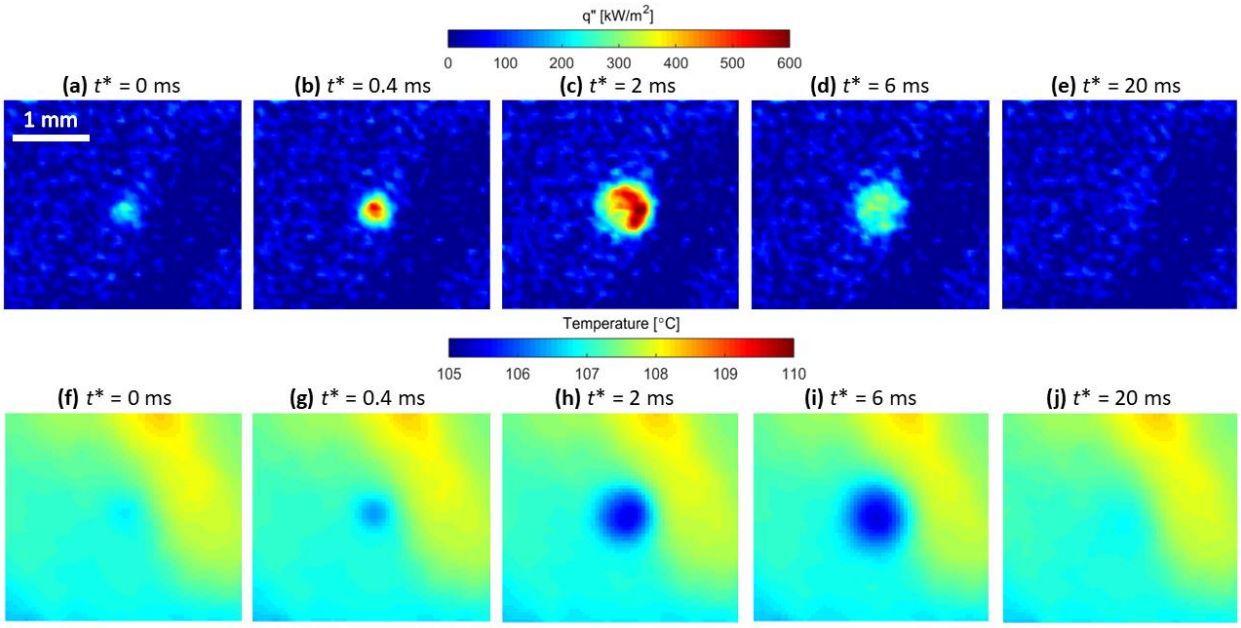


Figure 5. Heat flux and temperature distribution obtained from IR images during a bubble life cycle under a nominal heat flux of 30 kW/m².

4. CONCLUSIONS

In this study, we performed a first-of-its-kind simultaneous measurement of the temperature and velocity fields in the liquid phase and of the wall temperature during the nucleation and growth of single bubbles using simultaneous high-speed two-color laser induced fluorescence, particle image velocimetry and infrared thermometry. The spatiotemporally-resolved information obtained using the combination of these non-intrusive advanced optical diagnostics allowed us to shed light on the links between the different heat transfer mechanisms occurring during nucleate boiling. The temperature distributions obtained from 2cLIF and velocity fields from PIV revealed the mixing effect induced by the bubble growth and departure. Additionally, an accumulation of superheated liquid was observed in the vicinity of the pre-defined nucleation site. The wall heat flux distributions obtained from the post-processing of the IR images allowed us to verify the microlayer formation and to infer its thickness profile. There is an on-going effort to calculate the individual heat transfer contributions from the microlayer evaporation and superheated liquid layer to the vapor bubbles throughout its life cycle and under different nominal heat fluxes.

ACKNOWLEDGMENTS

This work was supported by the MIT International Science and Technology Initiatives (MISTI) Global Seed Funds, the Department for International Development (DFID) through the Royal Society-DFID Africa

Capacity Building Initiative, the Imperial College London Faculty of Engineering Dame Julia Higgins Postdoc Collaboration Fund and Chevron Corporation.

REFERENCES

1. J. Dirker, et al. “Thermal Energy Processes in Direct Steam Generation Solar Systems: Boiling, Condensation and Energy Storage.” *Frontiers in Energy Research*, **6**, (2019).
2. T.G. Theofanous, J.P. Tu, A.T. Dihn, T.N. Dihn, “The boiling crisis phenomenon: Part I: Nucleation and nucleate boiling heat transfer.” *Experimental thermal and fluid science*, **26**(6-7), pp. 775-792 (2002)
3. J. Coppeta, C. Rogers, “Dual emission laser induced fluorescence for direct planar scalar behavior measurements.” *Experiments in Fluids*, **25**(1), pp. 1-15 (1998)
4. R. Mathie, H. Nakamura, C.N. Markides. "Heat transfer augmentation in unsteady conjugate thermal systems–Part II: Applications." *International Journal of Heat and Mass Transfer*, **56**(1-2), pp. 819-833 (2013)
5. A. Charogiannis, J.S. An, C.N. Markides, “A simultaneous planar laser-induced fluorescence, particle image velocimetry and particle tracking velocimetry technique for the investigation of thin liquid-film flows.” *Experimental Thermal and Fluid Science*, **68**, pp. 516-536 (2015)
6. C.N. Markides, R. Mathie, A. Charogiannis, "An experimental study of spatiotemporally resolved heat transfer in thin liquid-film flows falling over an inclined heated foil." *International Journal of Heat and Mass Transfer* **93**, pp. 872-888 (2016)
7. W. Chaze, O. Caballina, G. Castanet, F. Lemoine, “Spatially and temporally resolved measurements of the temperature inside droplets impinging on a hot solid surface.” *Experiments in Fluids*, **58**(8), pp. 96 (2017)
8. J. Sakakibara, R.J. Adrian, “Whole field measurement of temperature in water using two-color laser induced fluorescence.” *Experiments in Fluids*, **26**(1-2), pp. 7-15 (1999)
9. V. Voulgaropoulos, G.M. Aguiar, O.K. Matar, M. Bucci, C.N. Markides, “Temperature and velocity field measurements of pool boiling using two-colour laser-induced fluorescence, infrared thermometry and particle image velocimetry”, *10th International Conference on Multiphase Flow*, Rio de Janeiro, Brazil, May 19–24, 2019 (2019).
10. V. Voulgaropoulos, P. Angeli, “Optical measurements in evolving dispersed pipe flows.” *Experiments in Fluids*, **58**(12), pp. 170 (2017)
11. A. Charogiannis, F. Denner, B.G. van Wachem, S. Kalliadasis, C.N. Markides, “Detailed hydrodynamic characterization of harmonically excited falling-film flows: A combined experimental and computational study.” *Physical Review Fluids*, **2**(1), pp. 014002 (2017)
12. M. Bucci, A. Richenderfer, G.Y. Su, T. McKrell, J. Buongiorno, “A mechanistic IR calibration technique for boiling heat transfer investigations.” *International Journal of Multiphase Flow*, **83**, pp. 115-127 (2016)
13. S. Narayan, A. Srivastava, S. Singh, “Rainbow Schlieren-based investigation of heat transfer mechanisms during isolated nucleate pool boiling phenomenon: Effect of superheat levels.” *International Journal of Heat and Mass Transfer*, **120**, pp. 127-143 (2018)